PERGAMON

International Journal of Solids and Structures 40 (2003) 1225–1242

INTERNATIONAL JOURNAL OF SOLIDS and STRUCTURES

www.elsevier.com/locate/ijsolstr

Microstructure-based stress analysis and evaluation for porous ceramics by homogenization method with digital image-based modeling

N. Takano [a,*], M. Zako [a], F. Kubo [a], K. Kimura [b]

[a] *Department of Manufacturing Science, Osaka University, 2-1 Yamada-oka, Suita, Osaka 565-0871, Japan*

[b] *Advanced Structural Design and Evaluation Group, Synergy Ceramics Laboratory, Fine Ceramics Research Association, 2-4-1 Mutsuno, Atsuta-ku, Nagoya 456-8587, Japan*

Received 3 October 2001; received in revised form 28 October 2002

Abstract

Multi-scale analysis using the asymptotic homogenization method is becoming a matter of concern for microstructural design and analysis of advanced heterogeneous materials. One of the problems is the lack of the experimental verification of the multi-scale analysis. Hence, it is applied to the porous alumina with needle-like pores to compare the predicted homogenized properties with the experimental result. The complex and random microstructure was modeled three-dimensionally with the help of the digital image-based modeling technique. An appropriate size of the unit microstructure model was investigated. The predicted elastic properties agreed quite well with the measured values. Next, a four-point bending test was simulated and finally the microscopic stress distribution was predicted. However, it was very hard to evaluate the calculated microscopic stress quantitatively. Therefore, a numerical algorithm to help understanding the three-dimensional and complex stress distribution in the random porous microstructure is proposed. An original histogram display of the stress distribution is shown to be effective to evaluate the stress concentration in the porous materials.

Keywords: Homogenization; Multi-scale analysis; Porous material; Microstructure; Ceramics; Digital image-based modeling; Stress analysis

1. Introduction

Multi-scale analysis for various advanced materials with microscopic heterogeneity has been one of the major topics in both computational mechanics and materials science. Among some computational methods for the multi-scale analysis, the asymptotic homogenization method has been successfully applied to the composite materials including polymer matrix composites (PMC) and metal matrix composites (MMC). Finite element method (FEM) is used to solve the partial differential equations derived by the

* Corresponding author. Tel.: +81-6-6879-7564; fax: +81-6-6879-7570.
E-mail address: takano@mapse.eng.osaka-u.ac.jp (N. Takano).

0020-7683/02/$ - see front matter © 2002 Elsevier Science Ltd. All rights reserved.
PII: S0020-7683(02)00642-X

homogenization method. This method was firstly developed by many applied mathematicians to solve linearly elastic problem and thermoelastic problem of heterogeneous media considering the microscopic properties (Sanchez-Palencia, 1980; Lions, 1981; Lene and Leguillon, 1982; Francfort, 1983). During the last decade, the efforts have been devoted to the enhancement of the homogenization method to solve many nonlinear problems that we encounter in the design, manufacturing and evaluation of composites (Guedes and Kikuchi, 1990; Takano et al., 2000).

One of the problems involved in the multi-scale analysis by the homogenization method is the lack of verification by comparison with experimental results. This sometimes becomes a hurdle when the materials scientists and engineers use this numerical method. In the application to the fiber reinforced PMC, Duvaut and Nuc (1983) compared the numerical prediction of the homogenized elastic constants of uni-directional fiber reinforced PMC with the conventional prediction rules. Bigourdan et al. (1991) showed the comparison with the experimental result in the prediction of the homogenized elastic property of woven fabric reinforced PMC. The authors (Takano et al., 2001a) verified the accuracy in the nonlinear problem. That is, the deep-drawing simulation of knitted fabric reinforced PMC was conducted using the homogenization method and the largely deformed microstructures were compared with the experimental result. In the above papers, the accuracy and the reliability of the homogenization method were shown. However, for other materials such as the porous ceramics studied in this paper, we can find no literature that proved the accuracy and the applicability of this method. Hence, in the first part of this paper, the elastic constants of a porous alumina with needle-like pores were measured and predicted by the homogenization method. For the practical modeling of the complex microstructure architecture, the digital image-based modeling technique and the voxel mesh are employed. The review of this technique is described later.

The second problem may be related to the assumption of the periodicity of the microstructure in the homogenization procedure. Whether the assumption of the periodicity is approval or not depends on the representative dimension of the microstructure and that of the macroscopic structure from the theoretical point of view. Moreover, the porous ceramics have random microstructure architecture, and therefore this assumption may cause some numerical error. It is shown in this paper that the periodic boundary condition compulsorily put on the microscopic unit cell model leads to the numerical error in the calculation of the microscopic stress.

The third problem is concerned with the evaluation of the predicted microscopic stress. No way has been shown to the materials scientists and engineers how to use the calculated microscopic stress in the design of advanced materials. One possibility may be the prediction of the microscopic damage propagation and the strength. In the analysis of damage propagation for woven fabric reinforced PMC, the microscopic stress was used with the failure criterion and the damage mechanics (Lene and Paumelle, 1992; Takano et al., 1999; Fish et al., 1999). However, the verification is limited to the qualitative agreement with the experimental data.

In many works on the enhancement of the homogenization method to the nonlinear problems such as the elasto-plastic problem (Jansson, 1992), creep problem (Wu and Ohno, 1999), large deformation problem (Takano et al., 2000) and buckling problem (Okumura et al., 2001; Saiki et al., 2001), the microscopic stress is of course used because the constitutive law is dependent on the stress. However, as mentioned above, we can find no literature that showed the verification except the authors' previous work (Takano et al., 2001a).

A problem lies essentially in the difficulty to understand the very complex stress distribution in the microstructure. The microscopic stress is rapidly changing in a small length scale depending on the heterogeneity. Moreover, we can hardly understand the three-dimensional distribution in the microstructure and the relation between the stress concentration and the heterogeneity. The current commercial postprocessors for finite element analysis do not have enough function to evaluate quantitatively the phenomena inside the material. Hence, in the latter part of this paper, a numerical method is presented to help evaluating the three-dimensional stress distribution quantitatively and understanding the relation between the stress concentration and the heterogeneity.

Table 1
Measured elastic constants of a porous alumina with 3.1% porosity ratio

Young's modulus (GPa)	366.0
Poisson's ratio	0.232

2. Measurement of elastic constants of porous alumina

We show first the material to be studied in this paper. The porous ceramics are believed to be useful for filters, heat insulators etc. with increased damage tolerance and reduced energy consumption. The design and the control of the microscopic pores are the key issue for the development of advanced porous ceramics. Therefore, the study on the effect of the microstructure on the macroscopic properties is essential. However, the classical rule of mixture is basically a function of the porosity ratio, but cannot take the microscopic geometry into account. The numerical approach using the multi-scale computational method is expected to provide the breakthrough in this field.

The aims of this paper are to verify the numerical prediction and to propose a method to evaluate the microscopic stress, as mentioned before. A test material made by alumina with needle-like pores was sintered by the addition of fugitive inclusions. The variations of the shape and the amount of the fugitive inclusions lead to the control of the pores. It was confirmed through observation by a scanning electron microscope (SEM) that no microscopic crack exists.

The Young's modulus and the Poisson's ratio were measured by pulse echo method for one of the sintered porous alumina. The porosity ratio of this material was 3.1% by measurement. The averaged length of the needle-like pores is approximately 150 μm, and the averaged diameter is approximately 10 μm. Note that the macroscopic component is usually in the scale order of 10 cm to 1 m, which means that the dimension of the microstructure is far small. Table 1 shows the experimental result. In this measurement, the isotropy was assumed for the macroscopic properties. It is compared with the computational result later in this paper.

3. Digital image-based modeling of microstructure

3.1. Overview

The finite element modeling of the complex three-dimensional microstructure of the heterogeneous materials such as composite materials and porous materials is a very cumbersome and troublesome procedure. For the practical use of the multi-scale analysis, the automatic mesh generation is essential. We can find some literatures (Shephard et al., 1995; Miravete et al., 1999) in which the complex textile composites are subdivided into finite element mesh using the tetrahedral elements. However, for the porous ceramics in this study, the microscopic geometrical information itself is unknown and must be captured experimentally, which costs so much.

Therefore, a digital image-based modeling technique is employed. It was firstly proposed by Hollister et al. (Hollister and Riemer, 1993; Hollister and Kikuchi, 1994) to model the porous microstructure of human bone in the biomechanical field. The detailed procedure is described in the application to the metal fiber reinforced MMC (Terada et al., 1997). Recently, we can find other applications to concrete (Nagai et al., 1998) and human bone (Adachi et al., 2000). The three-dimensional image of the inner microstructure is captured first by stacking the multiple cross-sectional images. The well-known pixel for two-dimensional image is enhanced to the voxel for three-dimensional case. The voxel is directly used as the cubic finite element, and consequently the voxel mesh is automatically generated.

One of the demerits using the automatic voxel meshing is that very large number of elements is required to express the complex microstructure architecture. This results in the very large-scale analysis. Therefore, an element-by-element preconditioned conjugate gradient (EBE-PCG) method is usually adopted to solve the stiffness equation (Hollister and Riemer, 1993). In this study, the diagonal scaling is used as the preconditioner, which is called EBE-SCG method.

Another problem is that the accuracy of the numerical results is really bad at the interface of dissimilar phases in the composite materials. It was investigated by Hollister and Riemer (1993) and the Gaussian filtering technique was used to obtain the stress at the interface. Nagai et al. (1998) developed an interface element especially for the voxel meshing. In this paper also, this problem is discussed later.

3.2. Application to porous alumina

Fig. 1 illustrates the flowchart of the digital image-based modeling procedure used in this study for porous alumina. In the digital image-based modeling, the resolution is important to ensure the quality of modeling and analysis (Terada et al., 1997). Here the resolution is equal to the voxel element size. To capture the image, the use of a micro-CT scanner is the most convenient way. However, the resolution of the general-use micro-CT scanner is limited to around 5–10 μm. It is insufficient to express the microstructure precisely because the averaged diameter of the needle-like pores of the target material in this study is approximately 10 μm. To this end, the porous alumina was polished precisely by every 2 μm, and the cross-sectional images were captured by a charge coupled device (CCD) camera as shown in Fig. 1. The accuracy in polishing was monitored so that the error is within ±0.25 μm. A typical cross-sectional image is

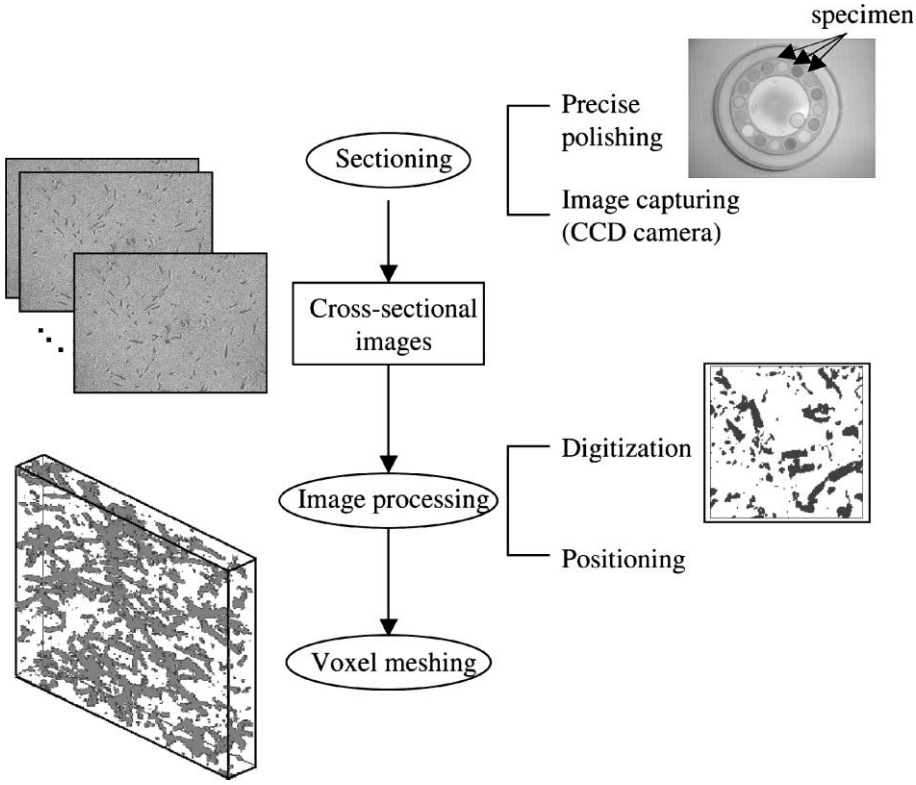

Fig. 1. Schematic of digital image-based modeling for porous alumina.

shown in Fig. 2. The demerit of this method is that very long time is needed for polishing, but the procedure is almost automated. In pursuit of the cost-effectiveness, we developed a specimen holder as shown in Fig. 1 so that many specimen can be polished at a time. The finer the resolution is, the better accuracy is obtained. However, the cost must be taken into account in the engineering sense to obtain accurate enough solution. The authors have so far investigated the accuracy of the voxel modeling in the homogenization analysis of fiber reinforced composite materials (Takano and Zako, 1995) and porous materials with spherical pores (Kimura et al., 2002). To this end, the resolution of 2 μm in this study was determined considering both the cost and the accuracy. In all the following numerical analyses, the voxel element size is 2 μm. However, as a numerical test, the voxel mesh with 4 μm element size was generated from the images with 2 μm resolution, and we found the relative error was approximately 2% between numerical results with 2 and 4 μm element sizes. Therefore, we can say the above-mentioned selection of the resolution that is equal to the voxel element size is adequate.

For the test material of porous alumina with 3.1% porosity ratio in Section 2, the reconstructed three-dimensional voxel mesh is shown in Fig. 3. Each voxel element size is 2 μm that is equal to the resolution in

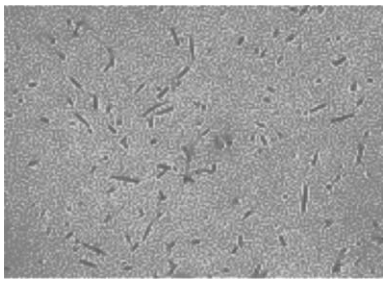

Fig. 2. Example of cross-sectional image of porous alumina with 3.1% porosity ratio.

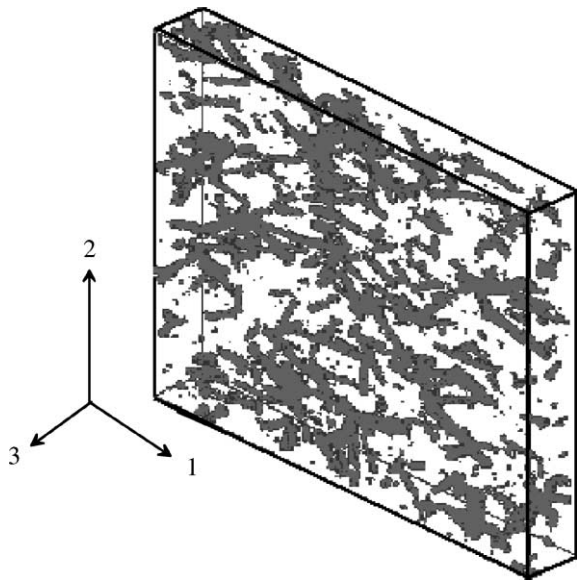

Fig. 3. Voxel mesh of porous alumina with 3.1% porosity ratio for the polished whole region (800 μm × 800 μm × 100 μm).

the image capturing process. The dimension of the polished whole region in Fig. 3 is 800 μm × 800 μm × 100 μm. Fifty-one cross-sectional images are stacked. In Fig. 3, only the pores are displayed. Here, both the solid alumina part and the pores are subdivided into voxel elements. This point is discussed later in Section 5.3. We can see that the needle-like pores are dispersed randomly, but in a macroscopic sense almost homogeneously. The measurement of the elastic constants in Section 2 was carried out for the whole region to obtain the macroscopic value in an averaged sense.

In the next section, the homogenization method is introduced and the unit cell modeling from the whole voxel data in Fig. 3 is discussed.

4. Homogenization and experimental verification

4.1. Outline of asymptotic homogenization method

In this paper, a linearly elastic problem is considered. The original formulation was presented in the early studies on the asymptotic homogenization method in 1980s (Sanchez-Palencia, 1980; Lions, 1981), and therefore only the outline of the formulation is described. However, the problem involved in applying this method to a material with random microstructure architecture is pointed out.

A macroscopic structure Ω is supposed to be made of a material that has the microscopic heterogeneity. If we can define a microscopic unit cell structure Y that can represent the global heterogeneity, the macroscopic properties can be defined as the volumetric average of the microscopic properties in the unit cell. The heterogeneous material can be replaced by the equivalent homogenized model. Now, it is assumed that the unit cell is repeated periodically.

Define the macroscopic scale $\boldsymbol{x}$ and the microscopic scale $\boldsymbol{y}$, and define the scale ratio ε that is usually a very small positive number so that $\boldsymbol{y} = \boldsymbol{x}/\varepsilon$. Write the displacement $\boldsymbol{u}$ asymptotically by means of the two-scale singular perturbation theory.

$$u_i(\boldsymbol{x}, \boldsymbol{y}) = u_i^0(\boldsymbol{x}) + \varepsilon u_i^1(\boldsymbol{x}, \boldsymbol{y}) \tag{1}$$

In this equation, u_i^0 is a macroscopic (or homogenized) displacement and u_i^1 is a perturbed term due to the microscopic heterogeneity. The former is proved to be a function of macroscopic scale only (Sanchez-Palencia, 1980; Lions, 1981).

We suppose that the traction t_i is applied on the boundary Γ and the body force is neglected. An elasticity tensor is denoted as E_{ijkh}. By taking the limit of $\varepsilon \to 0$ for homogenization, we finally obtain the decoupled microscopic and macroscopic equations. In this derivation, u_i^1 in Eq. (1) is assumed to be written by the following:

$$u_i^1(\boldsymbol{x}, \boldsymbol{y}) = -\chi_i^{kh}(\boldsymbol{y}) \frac{\partial u_k^0(\boldsymbol{x})}{\partial x_h} \tag{2}$$

where χ_i^{kh} is a characteristic displacement that is a periodic function with respect to the microscale. The microscopic equation to be solved for the unit cell Y under the periodic boundary condition is as follows:

$$\int_Y \left(E_{ijkh} - E_{ijmn} \frac{\partial \chi_m^{kh}}{\partial y_n} \right) \frac{\partial v_i^1}{\partial y_j} \, \mathrm{d}Y = 0 \quad \text{for } \forall v_i^1 \tag{3}$$

The existence and the uniqueness of the solution of Eq. (3) is shown in Sanchez-Palencia (1980) and Lions (1981). The macroscopic equation is derived as

$$\int_\Omega E_{ijkh}^H \frac{\partial u_k^0}{\partial x_h} \frac{\partial v_i^0}{\partial x_j} \, \mathrm{d}\Omega = \int_\Gamma t_i v_i^0 \, \mathrm{d}\Gamma \quad \text{for } \forall v_i^0 \tag{4}$$

where E^H_{ijkh} is the homogenized elasticity tensor that is also symmetric defined by

$$E^H_{ijkh} = \frac{1}{|Y|}\int_Y \left(E_{ijkh} - E_{ijmn}\frac{\partial \chi^{kh}_m}{\partial y_n}\right) \mathrm{d}Y \tag{5}$$

where $|Y|$ is the volume of the unit cell.

The microscopic stress can be calculated by the following equation:

$$\sigma_{ij} = \left(E_{ijkh} - E_{ijmn}\frac{\partial \chi^{kh}_m}{\partial y_n}\right)\frac{\partial u^0_k}{\partial x_h} \tag{6}$$

In this equation, $(\partial u^0_k/\partial x_h)$ is constant in the unit cell Y, and χ^{kh}_m is a periodic function, and thus the microscopic stress is periodic with respect to the microscale.

For some continuous fiber reinforced composites, we can find easily the periodicity of the microscopic unit cell (Takano et al., 2000). For the materials with random microstructure, it is known qualitatively that the size of the unit cell must be large enough to represent the global heterogeneity through two-dimensional analyses (Terada and Kikuchi, 1998; Moulinec and Suquet, 1998). However, no literature is found that proved it in the three-dimensional analysis because the three-dimensional analysis is usually very expensive (Smit et al., 1999). That is, the three-dimensional unit cell modeling for those materials is still a problem to be conquered not only in the homogenization procedure but also in the evaluation of the microscopic stress.

4.2. Unit cell modeling

As mentioned above, the extraction of the minimum size of the unit cell is required to reduce the computational cost, but it must be large enough to represent the global heterogeneity. In addition to determining the unit cell size, the location to extract the unit cell from the whole region in Fig. 3 is very important to ensure the objectivity. Now the influence of the voxel element size is discussed in Section 3.2.

Fig. 4 shows the unit cell models with 980 000 elements extracted from different location in the whole region shown in Fig. 3. The unit cell size is 280 μm × 280 μm × 100 μm. Each cubic voxel element size is 2 μm, which is discussed in detail in Section 3.2. Tables 2 and 3 show the calculated elastic constants by the two unit cell models. The Young's modulus of alumina is 404 GPa, and the Poisson's ratio is 0.239. The computational results show slight orthotropy. It is supposed that the orthotropy is due to the orientation of the fugitive inclusion in the press forming process. The pressure is applied for forming in the third direction in Figs. 3 and 4. The prediction tells that the Young's modulus in the third direction is lower, but is almost isotropic in the 1–2 plane. This is reasonable due to the orientation of the needle-like pores in the 1–2 plane as shown in the figures. What is important is that the predicted values by the two unit cell models agree well with each other. That is, the location of the unit cell is not influential on the computational results. Also, it is considered that the unit cell size is large enough to take the volumetric average.

To investigate further on the unit cell size, a larger unit cell model is studied as shown in Fig. 5. The unit cell size is 400 μm × 400 μm × 100 μm. The location to extract the unit cell is again different from the above smaller unit cell models. The predicted elastic constants are shown in Table 4. Comparing the values in Table 4 with those in Tables 2 and 3, it is concluded that the smaller unit cell models in Fig. 4 are large enough and cost-effective for the multi-scale analysis.

Note here that a standard personal computer (CPU: Pentium III, 500 MHz) is used for every analysis. The required core memory was 1 GB for the model with approximately one million elements, and 2 GB for two million elements by virtue of the EBE-SCG solver as mentioned in Section 3.1.

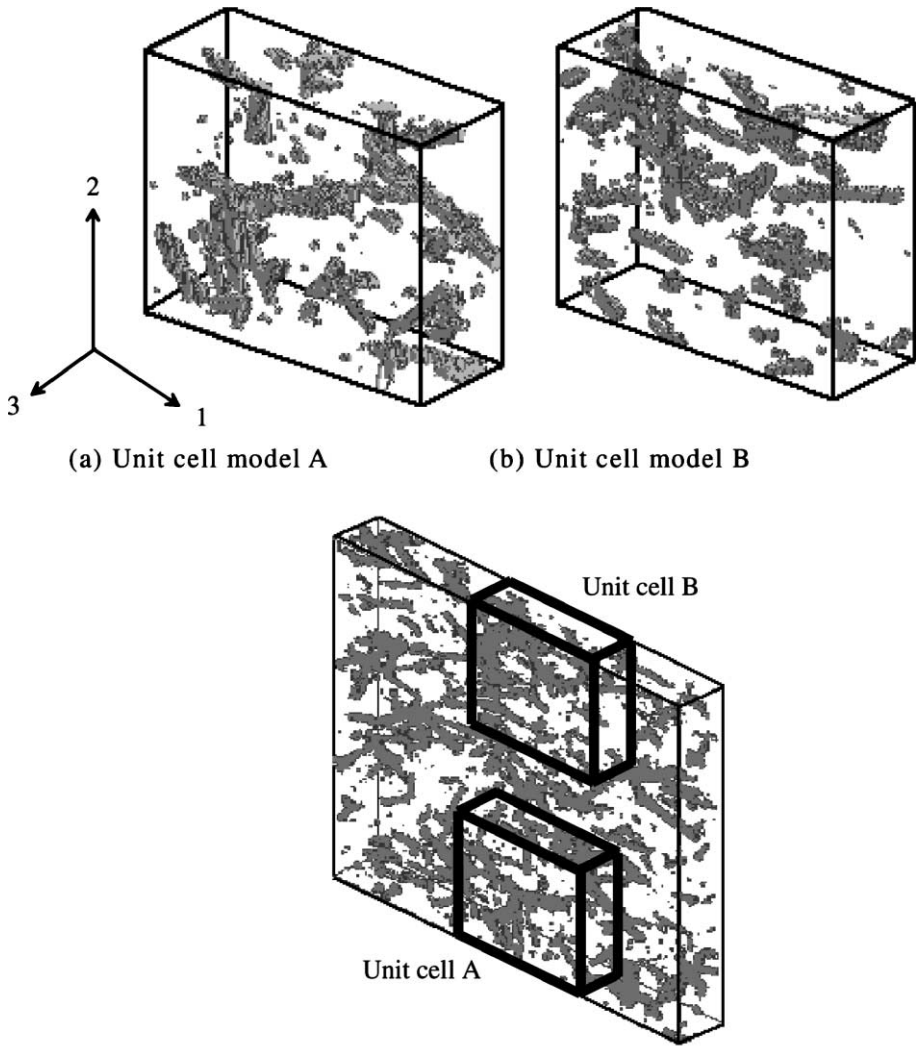

Fig. 4. Unit cell models with approximately one million voxel elements (280 μm × 280 μm × 100 μm).

Table 2
Predicted elastic constants by a unit cell model A with approximately one million voxel elements

E_{11}, E_{22}, E_{33} (GPa)	379.3	378.6	365.3
G_{23}, G_{31}, G_{12} (GPa)	149.3	149.5	153.0
ν_{21}, ν_{31}, ν_{32}	0.236	0.231	0.231

Table 3
Predicted elastic constants by a unit cell model B with approximately one million voxel elements

E_{11}, E_{22}, E_{33} (GPa)	381.4	378.8	364.0
G_{23}, G_{31}, G_{12} (GPa)	149.2	149.9	153.3
ν_{21}, ν_{31}, ν_{32}	0.236	0.229	0.231

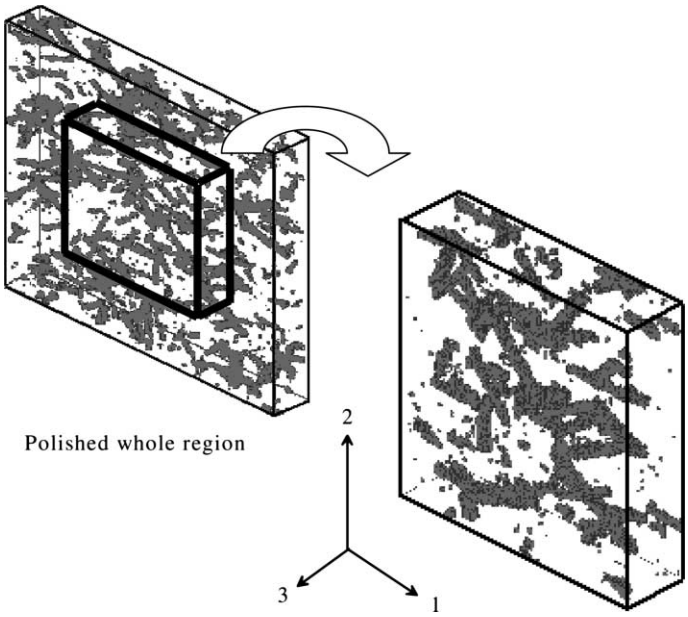

Fig. 5. Unit cell model with two million voxel elements (400 μm × 400 μm × 100 μm).

Table 4
Predicted elastic constants by a unit cell model with two million voxel elements

E_{11}, E_{22}, E_{33} (GPa)	381.3	377.1	362.0
G_{23}, G_{31}, G_{12} (GPa)	148.2	149.2	153.2
ν_{21}, ν_{31}, ν_{32}	0.235	0.228	0.231

4.3. Comparison with experiment

By the digital image-based modeling and the homogenization, it is found this porous alumina with needle-like pores shows slight orthotropy. However, as mentioned in Section 2, the measurement of the elastic constants was carried out in only the third direction in Fig. 3, which is the pressured direction during forming. Therefore, the Young's modulus in the third direction E_{33} was compared between the measurement (Table 1) and the numerical prediction (Tables 2–4). Obviously, the both agree quite well, and the relative error is approximately 1%.

The authors have proved so far that the same modeling and analysis strategy presented in this paper works well for porous alumina with spherical random pores with some porosity ratios ranging from 1% to 6% (Kimura et al., 2002). In that previous work, Hashin–Shtrikman's bound (Hashin and Shtrikman, 1963) can also predict well the homogenized properties because the shape of pores is simply spherical and because the porosity ratio is low. That is, the numerical prediction using the voxel modeling and homogenization method agreed well with both experimental results and the Hashin–Shtrikman's bound. However, the authors also found that the shape of the pores is much influential on the homogenized properties, and they can not be predicted by referring only the porosity ratio. Therefore, the present result for porous alumina with needle-like pores is advantageous over other related works.

Although the porosity ratio in this paper is low, other materials are now under preparation with higher porosity ratio and with obvious anisotropy. See also Beppu et al. (2001) for the advanced sintering

technology of highly porous ceramics. In such cases with anisotropy, bounds or other estimates may fail, whilst the present numerical analysis can be very effective.

5. Multi-scale analysis under four-point bending and microscopic stress evaluation

5.1. Problem's setting

In this section, a four-point bending problem of the porous ceramic with needle-like pores is studied, and both macroscopic and microscopic behaviors are analyzed using the homogenization method. Fig. 6 shows the specification of the four-point bending problem. A quarter part was modeled by hexahedral finite elements as shown in Fig. 7. The number of elements is 6000, and the number of nodes is 7776. A regular mesh is used, and each element size is 250 μm × 400 μm × 400 μm. The 1–2–3 coordinate system in Figs. 6 and 7 corresponds to that for the microstructures.

Two types of porous alumina with different porosity ratio were considered. The one has 3.1% porosity ratio as described in Section 4. Another material has higher porosity ratio, i.e., approximately 23%, but the contained needle-like pore is the same with the material with 3.1% porosity ratio. Fig. 8 shows the unit cell model of the material with 23% porosity ratio. Some examples of the cross-sectional meshes are shown in Fig. 9. Because the characteristic of the microscopic heterogeneity is the same between two porous materials except the porosity ratio, the same strategy was taken to determine the unit cell size. That is, in Fig. 8, each

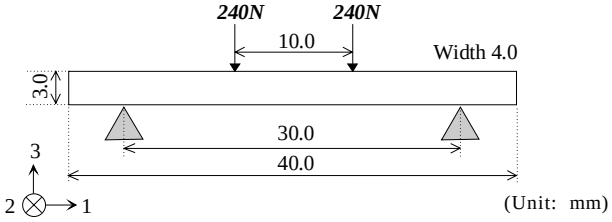

Fig. 6. Specification of four-point bending problem.

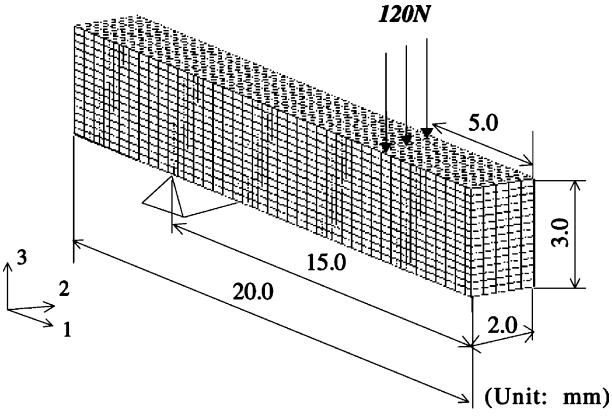

Fig. 7. Finite element mesh of macrostructure.

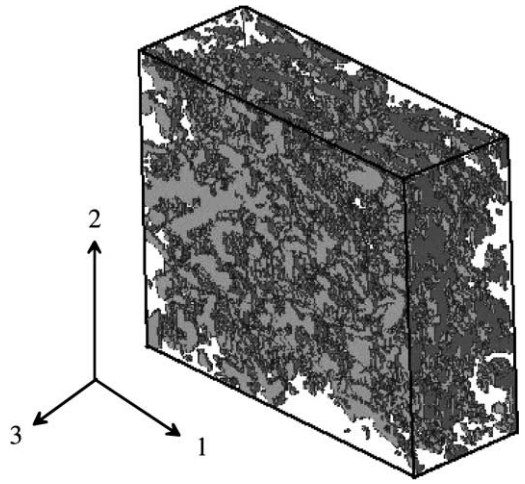

Fig. 8. Unit cell model of porous alumina with 23% porosity ratio.

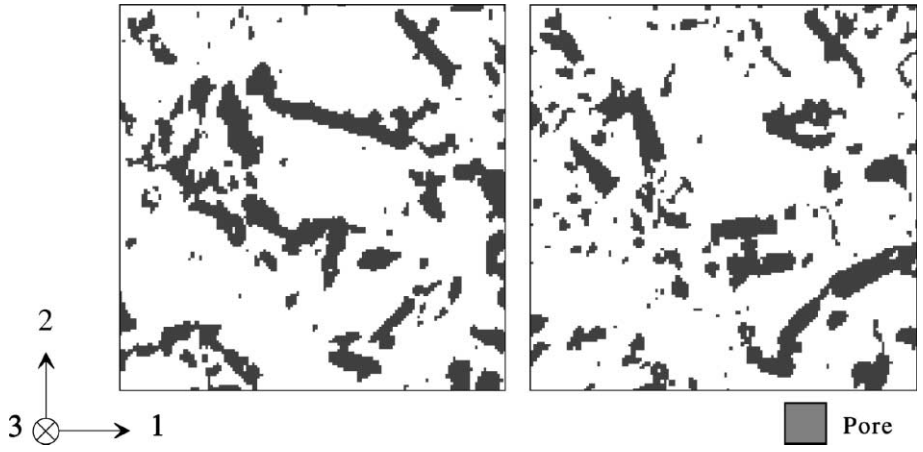

Fig. 9. Cross-sectional meshes of porous alumina with 23% porosity ratio.

voxel element size is 2 μm, the unit cell size is 280 μm × 280 μm × 100 μm, and the number of voxel elements is 980 000. The homogenized stress-strain matrix is obtained as follows:

$$E^{H}_{23\%} = \begin{bmatrix} 266.6 & 72.8 & 61.5 & 1.3 & -1.5 & 50.0 \\ & 265.4 & 61.7 & 5.6 & -0.4 & 1.1 \\ & & 194.6 & 3.6 & -0.7 & -0.2 \\ & & & 78.5 & -0.5 & -0.5 \\ & \text{sym.} & & & 80.1 & 2.1 \\ & & & & & 96.0 \end{bmatrix} \text{(GPa)} \tag{7}$$

The degree of the anisotropy is increased for the porous ceramic with high porosity ratio, which is due to the degree of orientation of the needle-like pores caused in the forming process. It is reasonable that the

oriented needle-like pores in the 1–2 plane results in the lower value of E_{3333}, which is supported by the rule of mixture for fiber reinforced composites.

5.2. Multi-scale stress analysis

Fig. 10 shows the macroscopic stress σ_{11}^{H} in the longitudinal direction of the beam made by porous alumina with 3.1% porosity ratio. In this analysis, the same load is applied for two types of materials, and consequently the macroscopic stress distribution is almost same between two materials with different porosity ratios.

The microscopic stress can be analyzed by Eq. (6). In this paper, the microscopic stress was analyzed at the position where the maximum tensile stress is seen as shown in Fig. 10. Note here that the thickness of the beam is 3 mm, and the dimension of the unit cell in the thickness direction (3rd direction) is 100 μm. Hence, the repeated number of periodicity is 30 in the thickness direction. Although the macroscopic strain in Eq. (6) is linearly distributed in the thickness direction, the assumption that the macroscopic strain is nearly constant in the unit cell may be accepted. If the number of periodicity is small, we need to use other computational method such as the finite element mesh superposition method (Takano and Zako, 2001b) or the higher-order theory.

Fig. 11 shows the microscopic stress σ_{11} for the unit cell model A in Fig. 4 with 3.1% porosity ratio. The stress concentration on the boundary surface of the unit cell is seen in Fig. 11, however this is due to the

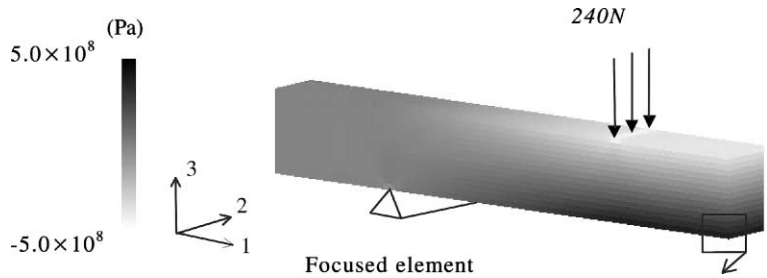

Fig. 10. Macroscopic stress distribution under four-point bending by a quarter model.

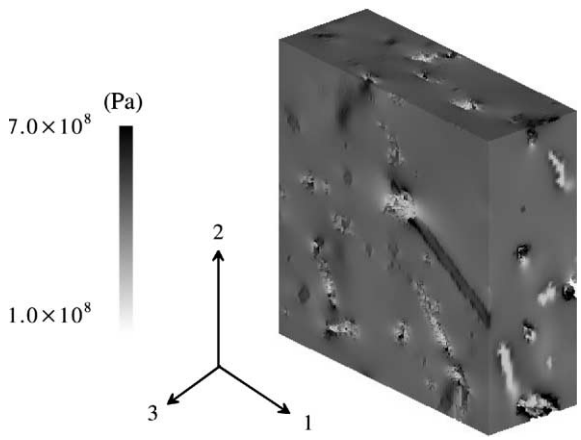

Fig. 11. Microscopic stress distribution in case of 3.1% porosity ratio for unit cell model A (280 μm × 280 μm × 100 μm).

assumption of the periodic boundary condition compulsorily put for the random microstructure architecture. Therefore, the boundary surface layer should be excluded in evaluating the microscopic stress. From the authors' preliminary studies (Kubo et al., 2000; Takano et al., in press), 10% in length from the boundary surface was omitted, and we use only the inner region (224 μm × 224 μm × 80 μm) for the stress evaluation as shown in Fig. 12. In the same manner, the microscopic stress distribution for the unit cell model B is shown in Fig. 13.

In case of porous alumina with 23% porosity ratio, the calculated microscopic stress σ_{11} in the inner region of the unit cell model is shown in Fig. 14. In this case with higher porosity ratio, the stress concentration is outstanding. Some of the cross-sectional views are shown in Fig. 15.

5.3. Evaluation of microscopic stress distribution

Only qualitative discussion may be possible by the three-dimensional and the cross-sectional displays of the microscopic stress distribution. Or it is even difficult to understand the relation between the stress concentration and the three-dimensional distribution of the needle-like pores. However, the quantitative evaluation is essential for the materials scientists and engineers.

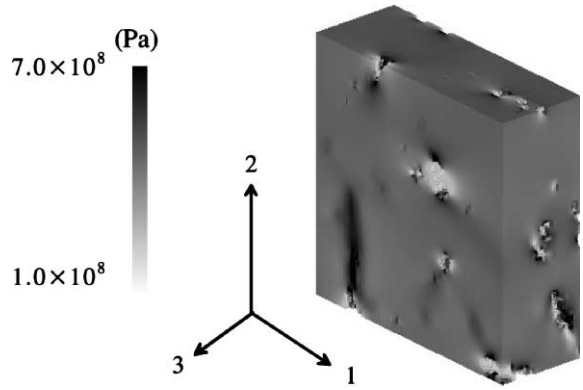

Fig. 12. Microscopic stress distribution in case of 3.1% porosity ratio in inner region of unit cell model A (224 μm × 224 μm × 80 μm).

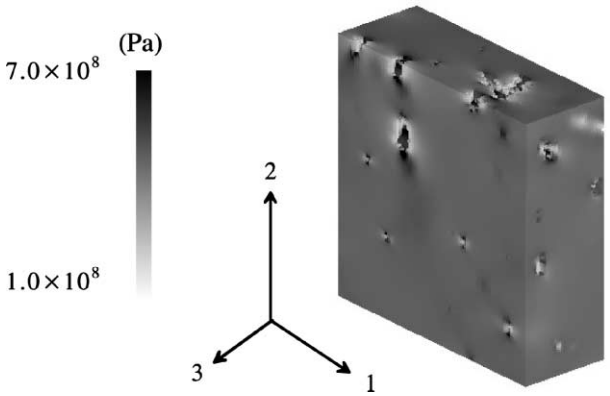

Fig. 13. Microscopic stress distribution in case of 3.1% porosity ratio in inner region of unit cell model B (224 μm × 224 μm × 80 μm).

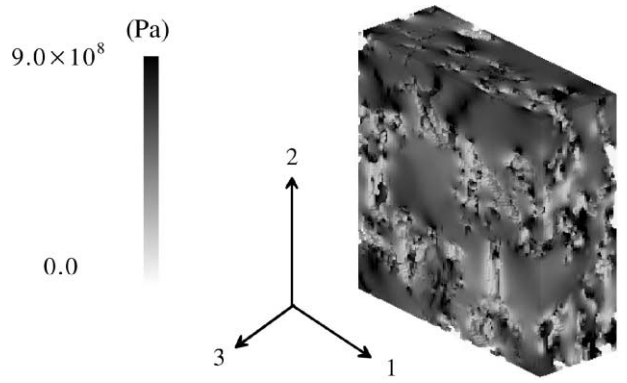

Fig. 14. Microscopic stress distribution in case of 23% porosity ratio (224 μm × 224 μm × 80 μm).

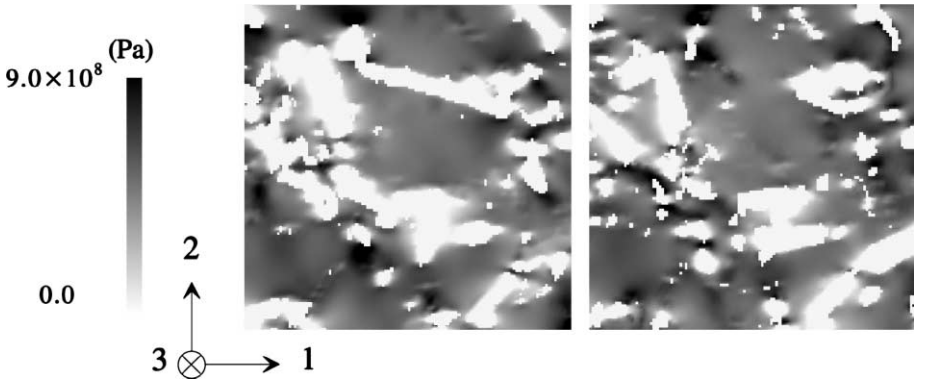

Fig. 15. Cross-sections for porous alumina with 23% porosity ratio.

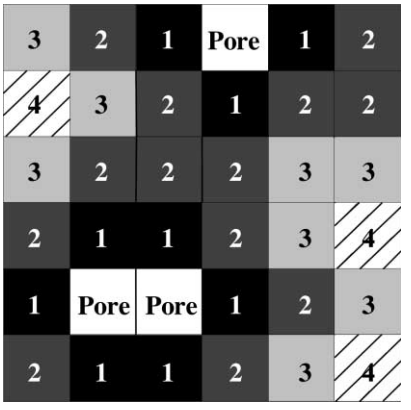

Fig. 16. Definition of distance for voxel mesh.

This paper proposes a histogram display of the microscopic stress distribution. Furthermore, the information of the distance from the nearest pore is plotted together in the histogram. The definition of the distance is shown in Fig. 16 for the two-dimensional case for simplicity, where the nature of the voxel mesh

is utilized. Because both solid part and pore are subdivided into voxel elements as described in Section 3.2 and consequently the voxel mesh is absolutely regular, it is very easy to calculate the distance from the nearest pore for all the voxel elements by this simple definition. Although the voxel meshing for the pore part leads to the increase of actual number of elements and to the decrease of computational performance, it is effective for this stress evaluation.

Fig. 17 shows the obtained histograms for the unit cell models A and B with 3.1% porosity ratio. Here, the longitudinal stress σ_{11} is shown for only the inner region of the unit cell models. The distance expressed by "d" in Fig. 17 is also plotted. The tendency is very close between the unit cell models A and B. It means that the location to extract the unit cell is not influential on the stress evaluation as well as the homogenization procedure. It is clearly found the high stress is observed at the neighborhood of the pores for small "d". As was mentioned in Section 3.1, the accuracy of the solution by the voxel mesh is bad at the interface ($d = 1$ in this study). Therefore, it is reasonable to neglect the stress for the elements with $d = 1$ in evaluation. Also, if we suppose that a point-wise stress is not usually used for evaluation or prediction of fracture, the exclusion of elements with $d = 1$ may not cause any problem. For instance, Terada and Kikuchi (1996) used an averaged stress in each phase for a two-phase material to determine numerically the phase distribution so that the mismatch of the stress is minimized. They did not pay any attention to the accuracy of the interface stress. However, excluding the elements with $d = 1$ will increase the accuracy. The proposed histogram makes such evaluation quite easy.

For the material with higher porosity ratio, Fig. 18(a) shows the histogram of microscopic stress σ_{11} in the whole unit cell region (280 μm × 280 μm × 100 μm). Fig. 18(b) shows that in only the inner region (224 μm × 224 μm × 80 μm). It is interesting that the high stress can be seen in Fig. 18(a) for the elements with $d \geqslant 6$ that are apart from the pores. Those elements are in the boundary surface layer of the unit cell. Because of the compulsory assumption of the periodic boundary condition, critical error is included for those elements. Indeed, in Fig. 18(b), the high stress can not be seen for the elements with $d \geqslant 6$. For the

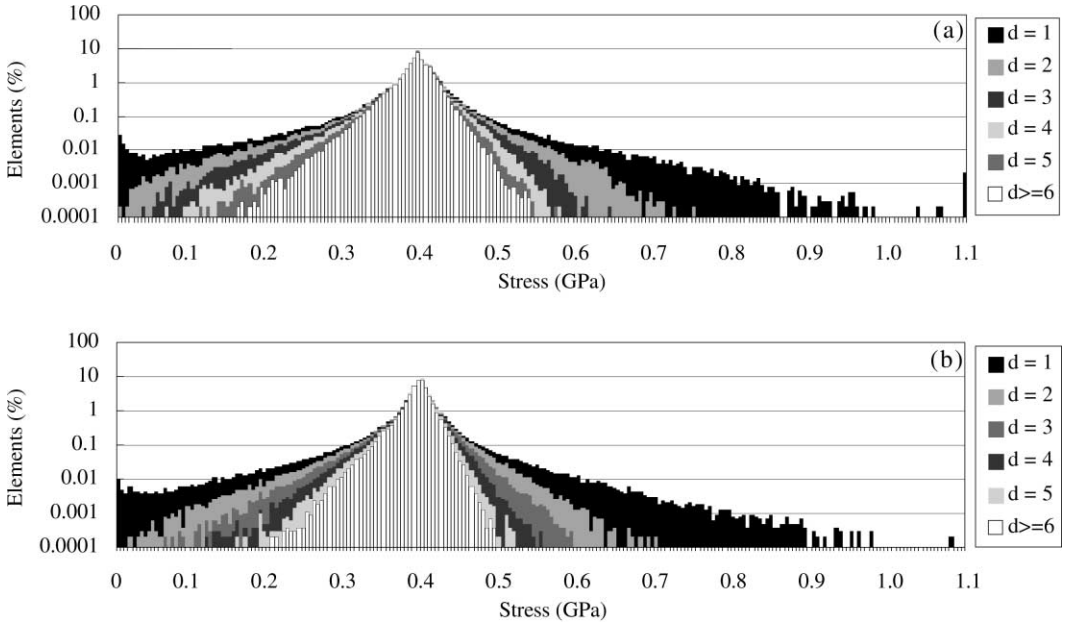

Fig. 17. Histogram display of microscopic stress distribution with distance information in case of 3.1% porosity ratio (224 μm × 224 μm × 80 μm). (a) Unit cell model A and (b) unit cell model B.

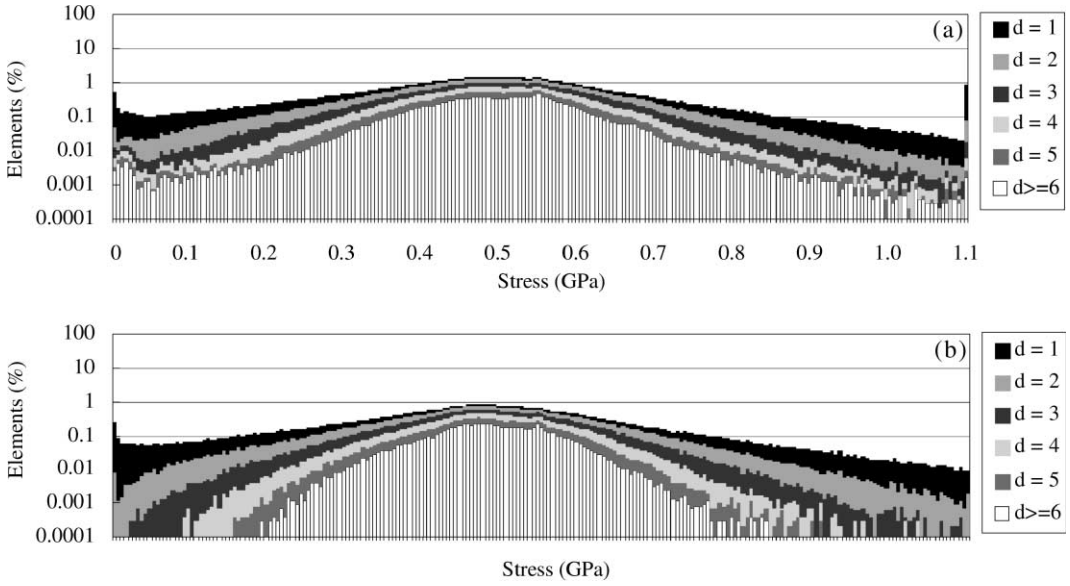

Fig. 18. Histogram display of microscopic stress distribution with distance information in case of 23% porosity ratio: (a) whole unit cell region (280 μm × 280 μm × 100 μm), (b) inner region of unit cell (224 μm × 224 μm × 80 μm).

materials with high porosity ratio that are often used for filters, the necessity to omit the boundary layer of the unit cell in evaluating the microscopic stress is again recognized.

Although the apparent peak was seen for low porosity ceramic in Fig. 17, the tendency is quite different in case of the high porosity ratio. In other words, the stress concentration is very localized in case of the low porosity ratio. Using the histogram, the region where the stress concentration occurs can be observed easily. Fig. 19 shows the regions where the microscopic stress σ_{11} is higher than 0.9, 0.6 and 0.5 GPa for the unit cell model A with 3.1% porosity ratio. It is found that every pore causes the stress concentration, but that strong stress concentration is localized near some pores probably due to the clustering of pores. We can

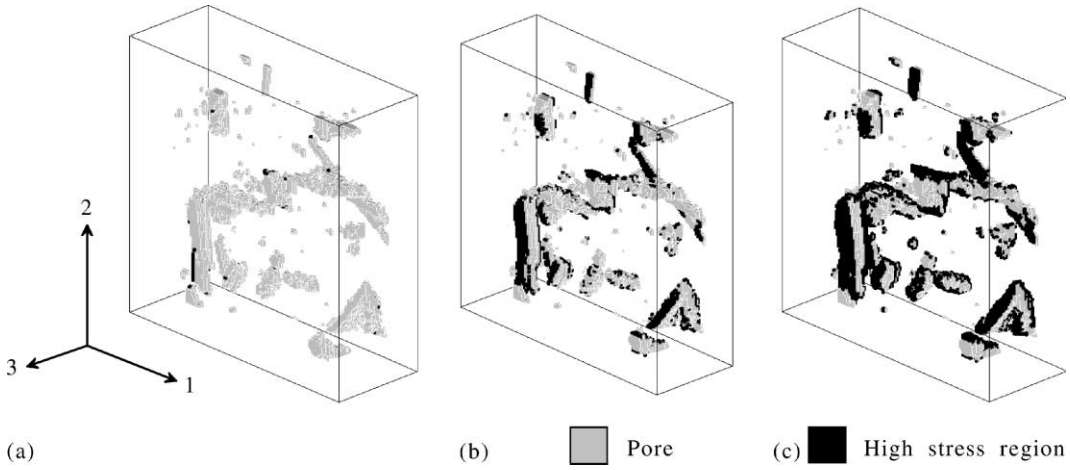

Fig. 19. High stress region for unit cell model A with 3.1% porosity ratio: (a) $\sigma_{11} \geqslant 0.90$ GPa, (b) $\sigma_{11} \geqslant 0.60$ GPa and (c) $\sigma_{11} \geqslant 0.50$ GPa.

say this is the only way to visualize the three-dimensional phenomena effectively and friendly, and it is much easier and more useful for us to understand than watching multiple cross-sectional views.

The proposed methods to evaluate the three-dimensional microscopic stress, i.e., a histogram with distance information and the visualization like Fig. 19, are not implemented in any currently existing software. But, we expect that it can accelerate the ongoing study on the fracture and micromechanism for various porous ceramics.

6. Conclusion

A multi-scale computational method using the homogenization method was applied to the porous alumina with 3.1% and 23% porosity ratios. The digital image-based modeling technique was used to generate the voxel mesh automatically. To express the microscopic heterogeneity in this study, the resolution of the voxel mesh was determined to be 2 μm. Using the unit cell model with 2 μm resolution and with approximately one million elements, the predicted homogenized elastic constants had only 1% error compared with the measured values. Both the practicality and the objectivity were assured. Next, the four-point bending problem was analyzed. To evaluate the microscopic stress quantitatively and to understand the relation between the stress concentration and the three-dimensional dispersion of needle-like pores, a histogram display with distance information from the nearest pore was proposed. The numerical error caused by the compulsory periodicity assumption for the random microstructure and by the voxel mesh was discussed. The histogram display was effective to recognize the local region where the stress concentration occurs. The four-point bending test as shown in Section 5 is now under preparation in order to investigate the correlation between the fracture in experiment and the calculated microscopic stress distribution.

Acknowledgements

This work has been supported by METI, Japan, as part of the Synergy Ceramics Project. Part of the work has been supported by NEDO.

References

Adachi, T., Tsubota, K., Tomita, Y., 2000. Mechanical remodeling simulation for cancellous bone using digital image-based model. Trans. Jpn. Soc. Mech. Eng. 66, 1640–1647 (in Japanese).

Beppu, Y., Ando, M., Ohji, T., 2001. Highly porous silicate ceramics fabricated by freeze-drying. In: Extended Abstracts Fifth Int. Symp. Synergy Ceram., Tokyo, Japan, pp. 164–165.

Bigourdan, B., Chauchot, P., Hassim, A., Lene, F., 1991. Homogenization for the design of cylindrical containers made of composite materials. In: Baptiste, D. (Ed.), Mechanics and Mechanisms of Damage in Composites and Multi-materials. Mechanical Engineering Publications, London, pp. 203–212.

Duvaut, G., Nuc, M., 1983. A new method of analysis of composite structure. In: Proc. Ninth European Rotor Craft and Powered Lift Aircraft Forum, Stresa, Italy, Paper no. 88.

Fish, J., Yu, Q., Shek, K., 1999. Computational damage mechanics for composite materials based on mathematical homogenization. Int. J. Numer. Meth. Eng. 45, 1657–1679.

Francfort, G., 1983. Homogenization and linear thermoelasticity. SIAM J. Math. Anal. 14, 696–708.

Guedes, J.M., Kikuchi, N., 1990. Preprocessing and postprocessing for materials based on the homogenization method with adaptive finite element method. Comput. Meth. Appl. Mech. Eng. 83, 143–198.

Hashin, Z., Shtrikman, S., 1963. A variational approach to the theory of the elastic behaviour of multiphase materials. J. Mech. Phys. Solids 11, 127–140.

Hollister, S.J., Kikuchi, N., 1994. Homogenization theory and digital imaging: a basis for studying the mechanics and design principles of bone tissue. Biotech. Bioeng. 43, 586–596.

Hollister, S.J., Riemer, B.A., 1993. Digital image based finite element analysis for bone microstructure using conjugate gradient and Gaussian filter techniques. In: Proc. Math. Methods in Medical Imaging II, The Int. Soc. Photo-Optical Instrumentation Eng., vol. 2035. San Diego, pp. 95–106.

Jansson, S., 1992. Homogenized nonlinear constitutive properties and local stress concentrations for composites with periodic internal structure. Int. J. Solids Struct. 29, 2181–2200.

Kimura, K., Takano, N., Kubo, F., Ogawa, S., Kawamoto, H., Zako, M., 2002. Image-based modeling and elastic analysis by the homogenization method for porous ceramics. J. Ceram. Soc. Jpn. 110, 567–575 (in Japanese).

Kubo, F., Takano, N., Zako, M., Kimura, K., 2000. Development of micro-macro coupled stress analysis system for ceramic components by homogenization method (part 1; modeling and analysis of polycrystalline material). In: Proc. JSME 13th Comp. Mech. Conf., Toyohashi, Japan, no. 00-17, pp.763–764 (in Japanese).

Lene, F., Leguillon, D., 1982. Homogenized constitutive law for a partially cohesive composite material. Int. J. Solids Struct. 18, 443–458.

Lene, F., Paumelle, P., 1992. Micromechanisms of damage in woven composite. In: Proc. ASME Energy Sources Tech. Conf., Houston, ASME PD, vol. 45, pp. 97–105.

Lions, J.L., 1981. Some Methods in the Mathematical Analysis of Systems and Their Control. Science Press, Beijing.

Miravete, A., Clemente, R., Castejon, L., 1999. Macromechanical analysis of 3-D textile reinforced composites. In: Miravete, A. (Ed.), 3-D Textile Reinforcements in Composite Materials. Woodhead Publishing, Cambridge, UK, pp. 100–150.

Moulinec, H., Suquet, P., 1998. A numerical method for computing the overall response of nonlinear composites with complex microstructure. Comput. Meth. Appl. Mech. Eng. 157, 69–94.

Nagai, G., Yamada, T., Wada, A., 1998. On a finite element procedure based on the real 3-dimensional image for concrete materials. J. Struct. Constr. Eng. 509, 77–82 (in Japanese).

Okumura, D., Ohno, N., Noguchi, H., 2001. Microscopic symmetric bifurcation analysis for cellular solids based on a homogenization theory of finite deformation (2nd report, application to in-plane buckling of hexagonal honeycombs). Trans. Jpn. Soc. Mech. Eng. 67, 925–932 (in Japanese).

Saiki, I., Terada, K., Ikeda, K., Hori, M., 2001. Estimate of periodicity of microstructure undergoing geometrical instability and multi-scale modeling of material instability. In: Proc. Conf. Comput. Eng. Sci., Tokyo, pp. 431–434 (in Japanese).

Sanchez-Palencia, E., 1980. Non-homogeneous media and vibration theory. In: Lecture Notes in Physics 127. Springer, Berlin.

Shephard, M.S., Beall, M.W., Garimella, R., Wentorf, R., 1995. Automatic construction of 3-D models in multiple scale analysis. Comput. Mech. 17, 196–207.

Smit, R.J.M., Brekelmans, W.A.M., Meijer, H.E.H., 1999. Prediction of the large-strain mechanical response of heterogeneous polymer systems: local and global deformation behavior of a representative volume element of voided polycarbonate. J. Mech. Phys. Solids 47, 201–221.

Takano, N., Kimura, K., Zako, M., Kubo, F., in press. Multi-scale analysis and microscopic stress evaluation for ceramics considering the random microstructures. Trans. Jpn. Soc. Mech. Eng. 68 (in Japanese).

Takano, N., Ohnishi, Y., Zako, M., Nishiyabu, K., 2000. The formulation of homogenization method applied to large deformation problem for composite materials. Int. J. Solids Struct. 37, 6517–6535.

Takano, N., Ohnishi, Y., Zako, M., Nishiyabu, K., 2001a. Microstructure-based deep-drawing simulation of knitted fabric reinforced thermoplastics by homogenization theory. Int. J. Solids Struct. 38, 6333–6356.

Takano, N., Uetsuji, Y., Kashiwagi, Y., Zako, M., 1999. Hierarchical modelling of textile composite materials and structures by the homogenization method. Model. Simul. Mater. Sci. Eng. 7, 207–231.

Takano, N., Zako, M., 1995. Microscopic simulation technique for composite materials using the homogenization method based on fixed grid. Trans. Jpn. Soc. Mech. Eng. 61, 589–594 (in Japanese).

Takano, N., Zako, M., 2001b. Microscopic stress analysis of heterogeneous media by finite element mesh superposition method. Trans. Jpn. Soc. Mech. Eng. 67, 603–610 (in Japanese).

Terada, K., Kikuchi, N., 1996. Microstructural design of composites using the homogenization method and digital images. Mater. Sci. Res. Int. 2, 65–72.

Terada, K., Kikuchi, N., 1998. Application of the asymptotic homogenization method for composites with irregular material configurations. Trans. Jpn. Soc. Mech. Eng. 64, 162–169 (in Japanese).

Terada, K., Miura, T., Kikuchi, N., 1997. Digital image-based modeling applied to the homogenization analysis of composite materials. Comput. Mech. 20, 331–346.

Wu, X., Ohno, N., 1999. A homogenization theory for time-dependent nonlinear composites with periodic internal structures. Int. J. Solids Struct. 36, 4991–5012.